Available online at www.sciencedirect.com
SCIENCE DIRECT®
Cement & Concrete Composites 26 (2004) 957–966
Cement & Concrete Composites
www.elsevier.com/locate/cemconcomp

Scanning electron microscopy imaging of hydraulic cement microstructure

Paul Stutzman

Building and Fire Research Laboratory, 100 Bureau Drive, Mail Stop 8621, National Institute of Standards and Technology, Gaithersburg, MD 20899, USA

Abstract

Use of the scanning electron microscope (SEM) with X-ray microanalysis allows study of clinker and cements; permitting measuring bulk phase abundance and surface areas of the phases, as well as bulk chemistry of constituent phases can be carried out. Direct imaging of hydraulic cements by SEM yields a more complete picture of both bulk and surface phase compositions. Mass percentages obtained by SEM imaging are in good agreement with percentages based upon QXRD and may differ significantly from those estimated by the Bogue calculations. The finer-grained phases (gypsum, tricalcium aluminate, and ferrite) show much higher surface areas per unit mass than the coarser-grained phases such as alite and belite. Such data are being applied to develop better relationships between the cement material properties and performance properties and to provide starting images for a cement hydration simulation model being developed at NIST.

Keywords: Cement; Clinker; Image processing; Image analysis; Microstructure; Phase; Scanning electron microscopy; X-ray powder diffraction

1. Introduction

Hydraulic cements comprise about 20% by volume of most concretes: their hydration products serve as a binder for the aggregate. Cement composition and fineness, along with other concrete constituents, influence fresh concrete properties such as rheology, heat evolution, setting, rates of strength development, ultimate strength, and color. The hydration products of cement (and on occasion, residual cement phases) affect concrete durability.

Cement clinker is manufactured from a finely-ground, homogenized blend of limestone, shale and iron ore sintered in a rotary kiln to temperatures of approximately 1450 °C: clinker nodules 3–20 mm in diameter are normally produced. The nodules are subsequently ground with gypsum, which serves to control setting, to a fine powder (<45 μm) to produce cement. Fig. 1 shows a representative clinker nodule.

LeChatlier [1] first examined thin sections of clinker using the then new petrographic microscope. About a decade later, petrographic investigations of A.E. Tornebohm named four crystalline phases alite, belite, celite, felite, in addition to a supposed glassy phase. Subsequent studies of clinker have utilized both transmitted light and reflected light on polished, etched surfaces and have sought to understand the connections between microstructure and performance properties. Reflected light microscopy is still widely used today and ASTM standard test method C 1356 is used for quantitative phase abundance determination [2].

Phase composition and texture (crystal size, abundance, and distribution) of clinker result from complex interactions of raw feed particle size, feed homogenization, and the heating and cooling regime. Mill grinding affects the cement microstructure through fracturing of the calcium silicates and interstitial phase crystals and, depending upon conditions, it may alter the form of calcium sulfate added at this stage to control cement setting. These features in turn influence the cement's hydration characteristics.

Phase abundance estimates are commonly derived from the bulk chemistry using the Bogue equation. Errors in phase abundance estimates were recognized early and derive in part from the variability of clinker phase chemistry relative to the assumed compositions, and from not accounting for minor constituents [4,5]. While

E-mail address: paul.stutzman@nist.gov (P. Stutzman).

0958-9465/$ - see front matter © 2004 Elsevier Ltd. All rights reserved.
doi:10.1016/j.cemconcomp.2004.02.043

Fig. 1. Nodule of portland cement clinker with a cut and polished face.

this approach has served the industry well, it does not consider the textural attributes of the clinker, i.e. features such as crystal size, phase distribution, and surface area, which will influence performance. In contrast, microscopy provides a direct means to observe and quantify microstructure features. Detailed information on clinker microscopy may be found in [6,7].

2. Phases in clinker and cement

Alite (tricalcium silicate, Ca_3SiO_5) forms the bulk of a clinker (40–70%, by mass) with crystal sizes up to about 150 μm. Alite generally displays a hexagonal crystal habit in cross section, with forms ranging from euhedral (clearly-defined crystal faces), to subhedral (poorly-defined crystal faces), to anhedral (no crystal faces). Minor oxide contents may range from about 3% to 4% by mass. Alite reacts rapidly with water and is responsible for much of the early-age (28 d) strength development [5,9] (Table 1).

Belite (dicalcium silicate, Ca_2SiO_4) forms 15–45% of a clinker, and displays a rounded habit with crystal sizes ranging from 5 to 40 μm. Normally the β polymorph is found in clinkers, although smaller amounts of, α, α'_H, and α'_l polymorphs may occur with minor oxides comprising up to 5%. Light microscopy of lamellar structures on etched specimens and X-ray powder diffraction data are useful for distinguishing the belite forms. Belite is less reactive than alite but does contribute to later-age strengths (>28 d). Upon hydration, both alite and belite form a poorly-crystallized calcium silicate hydrate (C–S–H) and well-crystallized calcium hydroxide.

Tricalcium aluminate, $Ca_3Al_2O_6$, comprises 1–15% of a clinker occurring as small 1–60 μm crystals exhibiting irregular to lath-like habit, filling the area between the ferrite crystals [6]. Tricalcium aluminate may occur as cubic or orthorhombic forms, and may contain up to 7% minor oxides. It is highly reactive with water.

Ferrite (tetracalcium aluminoferrite, $Ca_2(Al,Fe)O_5$), comprises between 0% and 18% of a clinker with crystal habits as dendritic, prismatic, and massive. Minor oxide content within ferrites may be up to 10% and ferrites exhibit variable reactivity with water. The ferrite and aluminate phases are sometimes referred to as the interstitial or matrix phases as they occur between, and appear to bind the silicate crystals.

Phases in lesser quantities, but still influential to performance, include periclase (MgO) and free lime (CaO). Periclase may exhibit a dendritic or equant crystal habit both within and between the other clinker constituents, ranging in size up to 30 μm. Free lime may occur as isolated rounded crystals or in masses with variable crystal size.

Alkali sulfates and calcium sulfates may also occur in clinker and are of interest since they have been found to affect hydration rates and strength development [10,11]. Increased alkali levels in clinker are considered potentially deleterious if alkali-susceptible aggregates are used in the concrete.

Miller and Tang [12] found arcanite (K_2SO_4), aphthitalite ($(Na,K)_2SO_4$), calcium langbeinite ($K_2SO_4 \cdot 2CaSO_4$), and soluble anhydrite ($CaSO_4$) in a sampling of North American clinkers, although the anhydrite was thought to be a byproduct of the laboratory extraction process. Taylor [5] lists additional alkali sulfate and sulfate phases such as thenardite (Na_2SO_4) in high Na/K clinkers and possibly anhydrite ($CaSO_4$) in some high-SO_3 clinkers. These phases form late in the clinkering

Table 1
Typical chemical compositions for the primary phases in cement clinkers. From [5]

	Na_2O	MgO	Al_2O_3	SiO_2	P_2O_5	SO_3	K_2O	CaO	TiO_2	Mn_2O_3	Fe_2O_3
Alite	0.1	1.1	1.0	25.2	0.1	0.1	0.1	71.6	0.0	0.0	0.7
Belite	0.1	0.5	2.1	31.5	0.1	0.2	0.9	63.5	0.2	0.0	0.9
Aluminate (cubic)	1.0	1.4	31.3	3.7	0.0	0.0	0.7	56.6	0.2	0.0	5.1
Ferrite	0.1	3.0	21.9	3.6	0.0	0.0	0.2	47.5	1.6	0.7	21.4
Aluminate (orthorhombic)	0.6	1.2	28.9	4.3	0.0	0.0	4.0	53.9	0.5	0.0	6.6
Aluminate (low Fe)	0.4	1.0	33.8	4.6	0.0	0.0	0.5	58.1	0.6	0.0	1.0
Ferrite (low Al)	0.4	3.7	16.2	5.0	0.0	0.3	0.2	47.8	0.6	1.0	25.4

process and generally are found along crystal perimeters within the voids [5]. Cements have one or more forms of calcium sulfate added upon grinding to control setting and, depending on its classification, may also contain calcite, slag, fly ash, or silica fume.

While it is important to know the bulk phase composition of a clinker or cement, the surface area of each phase will also affect cement performance, especially at early ages. The surface area of a constituent is influenced by the clinker texture and grinding characteristics, which may be studied by microscopy. A wide range of textures and compositions are possible in cement clinker, as illustrated by the three NIST Standard Reference Clinkers (Figs. 2–4). These clinkers were selected as representative of a wide range of North American clinker production with respect to phase abundance, crystal size and distribution. The images were obtained by backscattered electron imaging in a scanning electron microscope.

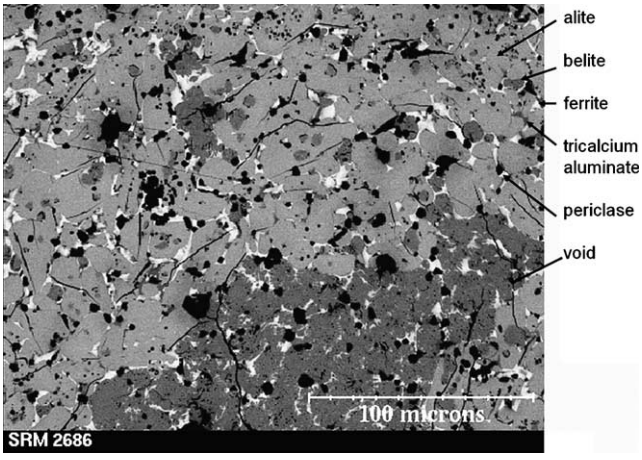

Fig. 2. NIST SRM 2686, SEM backscattered electron image.

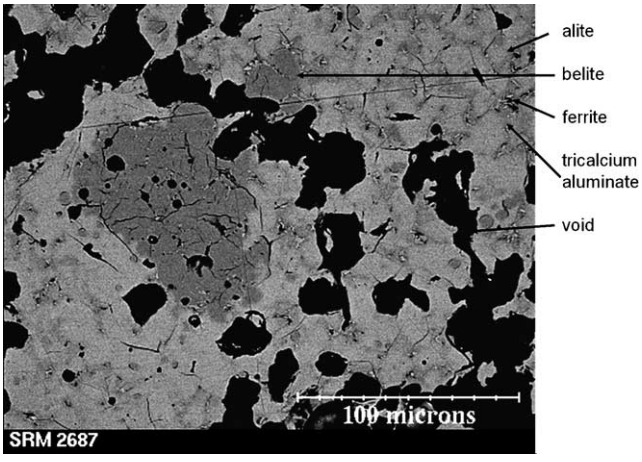

Fig. 3. NIST SRM 2687, SEM backscattered electron image.

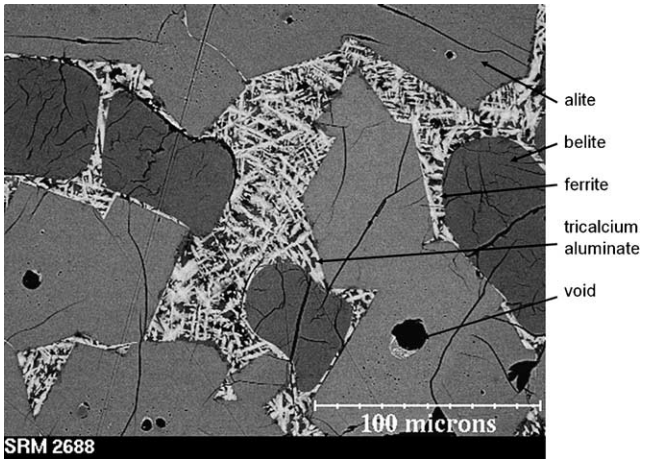

Fig. 4. NIST SRM 2688, SEM backscattered electron image.

Clinker 2686 (Fig. 2) is intermediate in crystal size and exhibits more heterogeneous phase distribution than the other clinkers. Alite appears as subhedral to anhedral crystals approximately 25 μm in size. Belite occurs in large clusters as rounded crystals about 15 μm in diameter, which often exhibits the internal lamellar structure. Ferrite occurs as medium- to fine-grained lath-like crystals. Aluminate is fine-grained and found between the ferrite crystals. Periclase occurs as equant crystals up to 15 μm in both the matrix and within some alite crystals.

Clinker 2687 (Fig. 3) exhibits fine crystal size and relatively homogeneous phase distribution, with the exception of belite and free lime, which occur as clusters within the microstructure. Alite occurs as anhedral grains approximately 12 μm comprising the bulk of the clinker. The matrix contains subhedral aluminate and fine-grained ferrite finely inter-grown and difficult to distinguish. Some of the pores contain alkali sulfates.

Clinker 2688 (Fig. 4) is the most coarsely crystalline of the clinkers, exhibiting the most homogeneous distribution of the constituent phases. Subhedral to anhedral alite crystals up to 110 μm form the bulk of the clinker. Belite occurs as rounded, evenly distributed crystals of about 35 μm diameter. Ferrite occurs with both lath-like and dendritic habit while aluminate crystals may be found between ferrite crystals.

3. Scanning electron microscopy imaging

Characterization of ground cements (as distinguished from clinkers) has been limited, due to its fine particle size and complex microstructure. Characteristic features such as crystal shape, occurrence within the microstructure, and etch color are all utilized for phase identification. The grinding reduces the particle size range to about 1–100 μm with a median size about

12 μm, diminishing the inter-phase relationship clues necessary for identification, and adding an additional phase, gypsum. Analyses using a light microscope generally limit sampling to the larger fragments as some etching techniques often used, may partially or completely dissolve the finer-sized particles. An alternative microscopy method, which avoids many of these difficulties is SEM imaging [13,14].

The SEM scans a high-energy electron beam across the surface of a specimen and measures one of a number of signals resulting from the interaction between the beam and specimen. Two particularly useful imaging methods are backscattered electron (BE) and X-ray (XR) imaging. Combining the BE and accompanying XR images via image processing allows their segmentation into the constituent phases of the microstructure. Once the image is segmented, it may be analyzed to extract information such as bulk phase abundance, phase surface area, and feature size.

Backscattered electrons are high-energy electrons (>50 eV) that have undergone multiple elastic scattering events within the specimen. The greater energy results in a larger interaction volume and lower spatial resolution compared to the secondary electron image. Contrast is generated by the different phases relative to their average atomic number. This is observed by the differential brightness in the image. The backscatter coefficient η is a measure of the backscattered electron fraction and, for a pure element of atomic mass Z, may be estimated from [16] and is shown graphically in Fig. 5.

The backscattered electron coefficient of a multi-element phase is estimated using the mass fractions (C_i) and η values for each constituent:

$$\eta = \sum_i C_i \eta_i \tag{1}$$

Contrast between constituents may be calculated as:

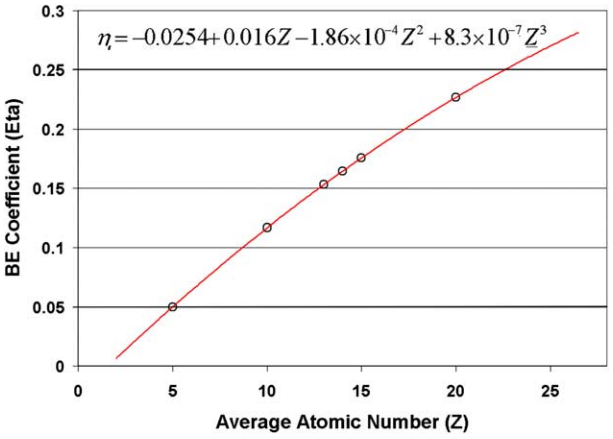

Fig. 5. Backscattered electron coefficient versus atomic number (Z), from Goldstein et al. [16].

$$C = \frac{(\eta_2 - \eta_1)}{\eta_2} \tag{2}$$

Table 2 is a list of some phases from clinker and cement, in descending order of their gray level intensity. The 6.8% contrast between alite ($\overline{Z} = 15.06$) and belite ($\overline{Z} = 14.56$) is relatively strong; that between belite and cubic tricalcium aluminate ($\overline{Z} = 14.34$), at 1.5%, is generally too weak to distinguish these constituents. If the contrast between phases is so weak that it precludes discrimination, they are usually chemically distinct, and therefore X-ray imaging can be used to distinguish them from each other.

Characteristic X-rays are another signal produced as a result of the electron beam–specimen interaction. X-ray microanalysis systems generally employ an energy-dispersive detector. The X-ray signal is used to determine which elements are present and in what concentration, and graphical display of relative concentrations through line scans and X-ray imaging of element

Table 2
Clinker and cement phases, composition, cement chemist notation, densities, average atomic number and backscattered electron coefficient ranked according to relative SEM BE image brightness

Phase	Composition	Notation	Density (Mg/m^3)	$\overline{Z}$	η
Ferrite	$Ca_2(Al,Fe)_2O_5$	C4AF	3.77	16.65	0.1860
Free lime	CaO	C	3.32	16.58	0.1882
Alite	Ca_3SiO_5	C3S	3.13–3.22	15.06	0.1716
Belite	Ca_2SiO_4	C2S	3.28–3.31	14.56	0.1662
Arcanite	K_2SO_4	$K\overline{S}$	2.67	14.41	0.1652
Aluminate—cub.	$Ca_3Al_2O_6$	C3A	3.04	14.34	0.1639
Aluminate—ort.	$NaCaAl_3O_9$	C3A	2.56	13.87	0.1588
Aphthitalite	$(Na,K)_2SO_4$	$KN\overline{S}$	2.7	13.69	0.1577
Syngenite	$K_2Ca(SO_4)_2H_2O$	$CK\overline{S}2H$	2.6	13.60	0.1556
Anhydrite	$CaSO_4$	$C\overline{S}$	2.98	13.41	0.1535
Bassanite	$2CaSO_4 \cdot H_2O$	$C\overline{S}H$	2.7	13.03	0.1489
Gypsum	$Ca(SO_4) \cdot 2H_2O$	$2C\overline{S}H$	2.32	12.12	0.1381
Thenardite	Na_2SO_4	$N\overline{S}$	2.66	10.77	0.1249
Periclase	MgO	M	3.58	10.41	0.1213

spatial distribution and relative concentrations. Mass concentration to a few tenths of a percent can be detected for some elements. The relative accuracy of quantitative analysis (using certified standards, and solid, homogeneous specimens) is about ±20% for concentrations around 1%, and about ±2% for concentrations greater than 50%. More details on X-ray microanalysis may be found in [16].

3.1. Sample preparation

SEM imaging using backscattered electrons and X-rays requires a polished specimen for optimum performance [17]. Approximately 25 g of the cement powder are blended with an epoxy resin (Epotek 353ND [1,2]) to form an extremely viscous paste. The mixture is pressed into a plastic mold (32 mm diameter) and cured at room temperature for 24 h. The cured specimen is then cut to obtain a plane surface for imaging and saw marks are removed using 600 grit followed by 1200 grit sandpaper. Final polishing is done on a lap wheel with (9, 3, 1, and 0.25) micrometer diamond paste for 120 s each. After each polishing, the specimen is cleaned using a clean polishing cloth. The final polished specimen is coated with carbon to provide a conductive surface for SEM imaging.

3.2. Image acquisition

The specimen is placed in the SEM chamber, and images collected for the backscattered electrons and selected elements. Typical accelerating voltage, probe current, and collection times for the images are 12 kV, 3 nA, and 2.5 h, respectively. An accelerating voltage of 12 kV is used to balance the need for high spatial resolution and low X-ray absorption of the lighter elements, and to provide a satisfactory over-voltage for excitation of heavier elements such as iron.

Brightness and contrast settings are adjusted so that the brightest constituents (ferrite) are at the peak-white gray level, and the darker constituents (periclase) are close to black. Image averaging further reduces noise through collection of multiple images, facilitating discrimination from the BE image. X-ray images are collected for elements Ca, Si, Al, Fe, S, K, Na, and Mg. Because these XR images are collected simultaneously with the backscattered electron image, the image set may be combined to classify the mineral phase present at each location (pixel) in the two-dimensional image. Imaging magnification of 500× provides a resolution of 0.5 μm per pixel (512 pixels by 408 pixels in size) which is approximately the resolution of the X-ray images. Data from replicate samples indicate that about four arbitrarily-selected fields of view provide a reasonably representative sampling for many cements. The figures used to illustrate the procedure in this paper were collected at a greater magnification (1000×) to provide clarity in publication.

3.3. Image processing

Digital images are made up of pixels, each of which may have one of 256 levels of intensity. The SEM images are monochrome as they reflect the electron or X-ray flux at each pixel. They can be pseudo-colored to improve visual discrimination of constituents through changes in image intensity. Image analysis is actually composed of two tasks; (1) image processing to enhance details, feature differences, and isolate constituent phases and, (2) image analysis to perform measurements on those features. Measurements may include area fraction, surface area, size, and distribution.

Fig. 6 shows high-magnification BE and XR images of polished cement particles embedded in an epoxy. The individual element density maps for Ca, Si, Al, Fe, S, K, Mg, are displayed with the backscattered electron image in the lower-right corner.

The first step in processing uses filtering operations to reduce random noise in the X-ray images. The median filter is useful to accomplish this while retaining edge details. The BE image noise is generally low enough that random noise poses fewer problems for segmentation. Given this, emphasis for phase segmentation is given to this image and the X-ray images are used only when necessary.

3.4. Segmentation strategies

Segmenting the image set utilizes standard image processing arithmetical and logical operations to code criteria for constituent identification based upon the BE and XR image intensities. For example, in the backscattered electron image, the ferrite phase is brightest, and is discriminated via image processing using the operation: 245 if (BE_IMAGE > 240) ELSE 0. This creates a binary image with intensity 245 if a pixel in the BE image is greater than 240 while zeroing pixels not meeting that criteria. If free lime is present, it may overlap the BE intensities of ferrite. In this case, high signal levels in the calcium image and bright BE image regions may be combined to effect the separation.

Alite is second brightest component and can usually be discriminated using the BE image. The belite gray level range generally overlaps that of tricalcium

[1] Certain trade names and products are identified to adequately specify the experimental procedure. In no case does such identification imply recommendation or endorsement by the National Institute of Standards and Technology, nor does it imply that the products are necessarily the best available for the purpose.

[2] Epotek 353 ND, Epoxy Technology, Billerica, MA, http://www.epotek.com.

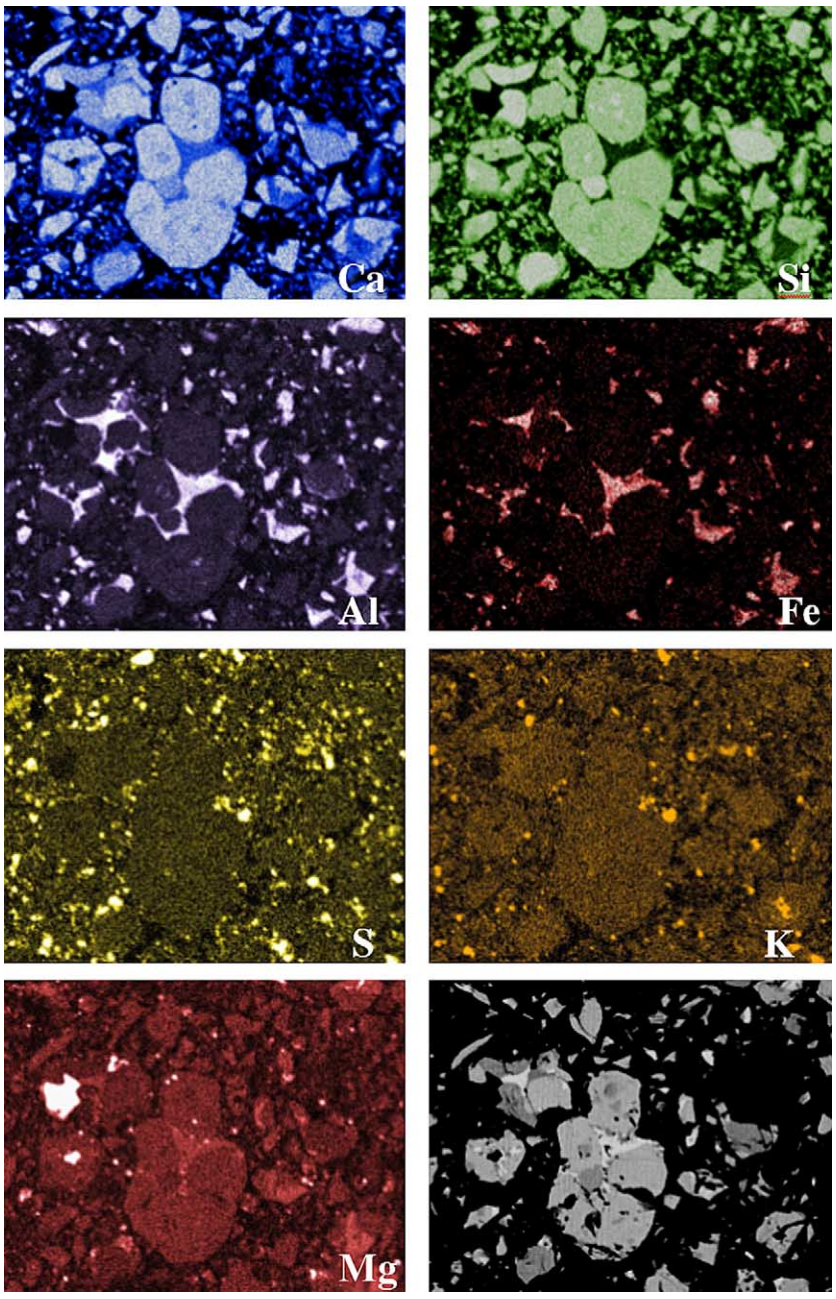

Fig. 6. SEM, X-ray and BE (lower right) images of a cement. Field width, 150 μm.

aluminate. This initially appeared to provide a problem but, as tricalcium aluminate and belite are chemically distinct, the aluminum XR image is used to threshold both tricalcium aluminate and ferrite; subsequently the ferrite portion is subtracted using the ferrite image created as described above. The resulting tricalcium aluminate binary may then be subtracted from the belite/tricalcium aluminate composite image to provide an image of belite distribution.

Alkali sulfates are regions of K and S, or Na and S, or K and Na and S, depending upon the phases present. Calcium sulfates (gypsum, bassanite, anhydrite) are the S-bearing regions not associated with the alkalies. Re-examination of these regions in the BE image may allow further discrimination into the calcium sulfate forms based upon their BE intensities. Periclase is identified by a high Mg content and dark backscattered image signal. Supplementary materials are taken on a case-by-case basis utilizing data collected on their chemistry. Slag has a high Mg and moderate Ca, calcined kaolin has aluminum and silicon, while multi-component fly ashes are generally more complex.

Fig. 7(upper) provides images of the segmented phases for alite, belite, tricalcium aluminate, ferrite, gypsum, periclase, and alkali sulfate. In the center is the backscattered electron image, for comparison, and be-

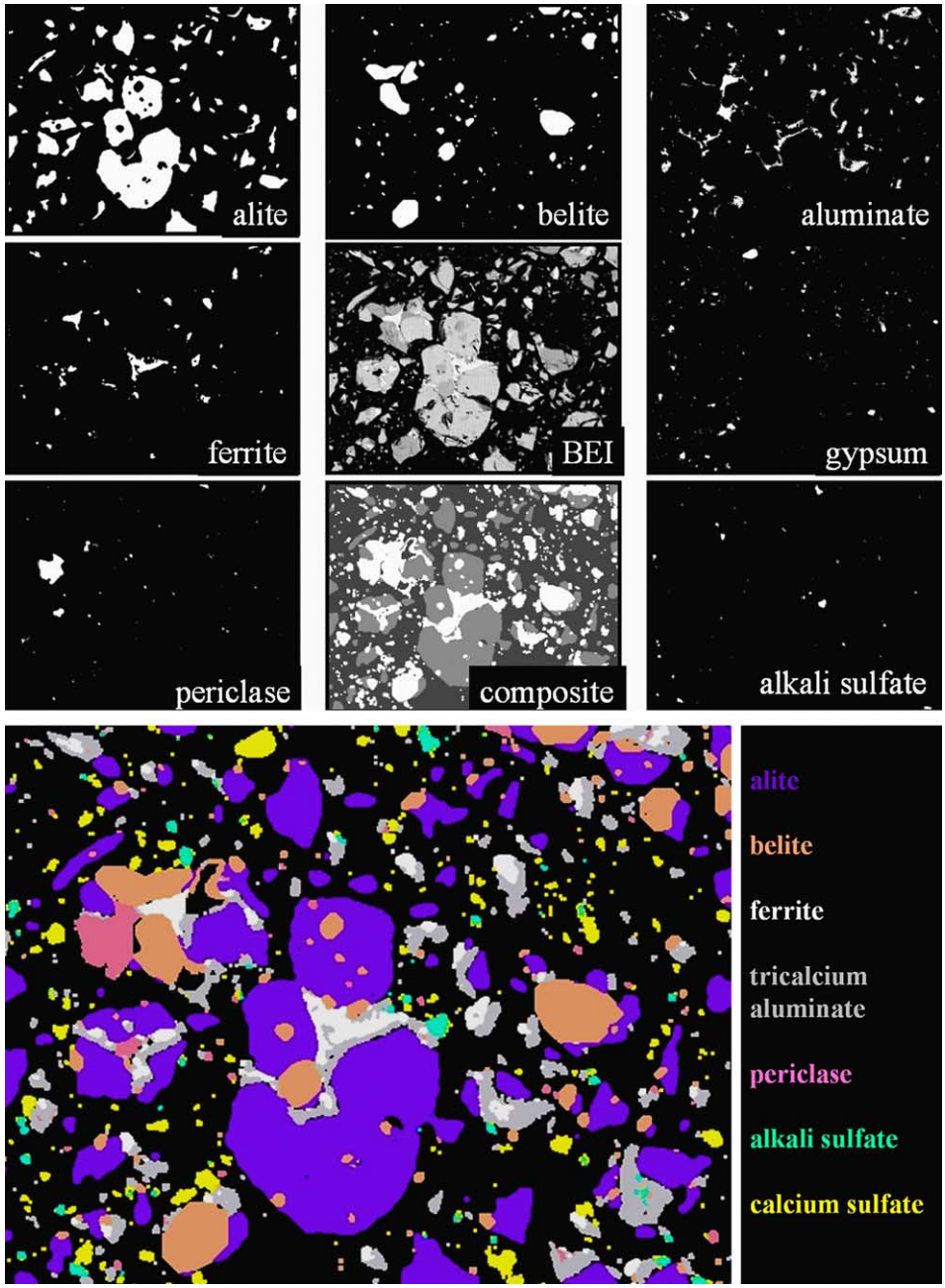

Fig. 7. Segmented phases (upper image set) and merged into a composite image ready for area analysis (lower). Field width, 150 μm.

low this is a composite image showing locations and boundaries of all the phases. The lower portion of Fig. 7 shows the composite image at a larger scale reconstructed so that each of the phases is displayed in its own false color. The black areas are epoxy-filled spaces.

3.5. Stereological analysis

Quantitative microscopy dates to the mid-19th century and is based upon the realization that in a randomly-selected sampling of a polished section, the ratio of the area of a mineral to that of all minerals is a consistent estimate of its volume fraction [18]. Similarly, the perimeter area fraction in two dimensions provides an estimate of the surface area exposure of the constituent phases.

With the digital SEM images, use of the entire image allows measurements of the perimeter and phase surface areas after the image has been segmented into the constituent phases. Image analysis operations on the composite image sum the number of pixels for each discrete phase color to measure the area fraction of each constituent. Similarly, the outer layer of pixels may also be summed to provide an estimate of each phase's surface

area. For comparison to other data, such as X-ray powder diffraction, mass percentages may be calculated by multiplying the volume fractions by the specific gravity of the corresponding clinker phase, and normalizing the totals to 100%.

4. Cement example

The Cement and Concrete Reference Laboratory (CCRL) portland cement proficiency sample program for inter-laboratory testing distributed its first sample in 1936 for chemical and physical testing. A program is underway at NIST to examine performance properties relative to compositional and physical parameters of these cements. These images are also utilized within the Virtual Cement and Concrete Testing Laboratory (VCCTL) where computer-based simulation models are used to predict cement and concrete performance properties [19].

CCRL cement #142 was selected for analysis in this example. A graphical display of phase abundance averages versus the number of fields shown in Fig. 8. For this cement, it is apparent that four fields provide a good estimate of phase abundance.

Fig. 9 compares three separate phase composition estimates based upon SEM imaging and X-ray powder diffraction (QXRD). Table 3 provides individual field estimates of the SEM data and that by the Bogue calculation as provided in ASTM C-150. The SEM estimates of both the bulk and surface phase fractions are expressed as mass fractions for comparison. The QXRD data are based upon a bulk cement and salicylic acid–methanol extraction data refined using Rietveld analysis [20].

Compared to the XRD data, the Bogue estimates (Table 3) are low for alite and high for belite, aluminate and ferrite. They do not provide an estimate for periclase, alkali sulfate or gypsum. In contrast, in Fig. 9 it is seen that the SEM bulk and the QXRD data generally show agreement within the error bars of their estimates.

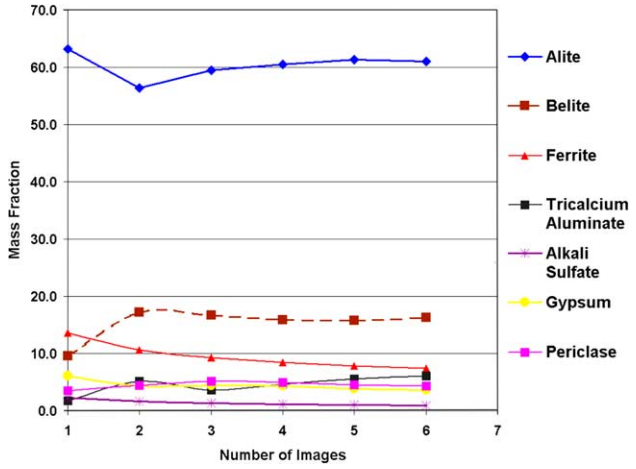

Fig. 8. Cumulative mass fraction averages versus number of fields shows the estimates stabilize after four fields.

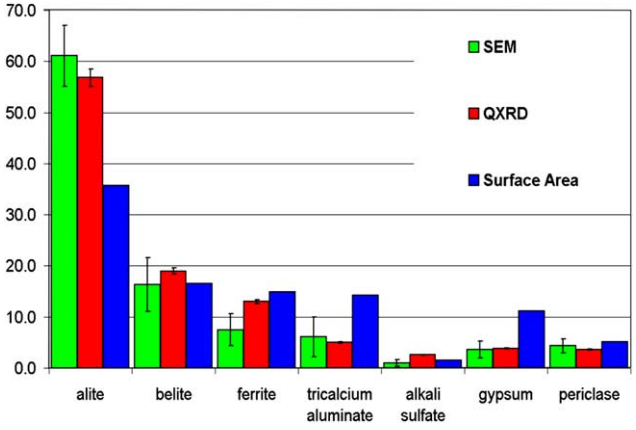

Fig. 9. Comparison of mass fraction estimates for CCRL 142 based upon bulk SEM imaging, quantitative X-ray powder diffraction, and surface area fraction by SEM.

The surface phase fractions are of interest in early-age cement hydration as they are often quite different from

Table 3
Mass fraction estimates of CCRL 142 cement based upon SEM imaging of six fields of view at 500× magnification. ASTM C-150 estimates of bulk phase abundance are provided in the bottom row

	Alite	Belite	Ferrite	Tricalcium aluminate	Alkali sulfate	Gypsum	Periclase	Quartz
Field 1	63.2	9.6	13.6	1.8	2.2	6.1	3.5	0.0
Field 2	49.6	24.9	7.6	8.6	1.1	2.6	5.5	0.1
Field 3	65.6	15.8	6.6	0.5	0.5	4.6	6.4	0.0
Field 4	63.6	13.3	5.8	7.6	0.6	4.1	4.6	0.4
Field 5	64.8	15.3	5.4	9.2	0.7	1.4	3.0	0.1
Field 6	59.7	19.2	5.7	8.9	0.5	2.9	3.2	0.0
Average	61.1	16.3	7.5	6.1	0.9	3.6	4.3	0.1
Std. dev.	6.0	5.3	3.1	3.9	0.7	1.7	1.4	0.2
ASTM C-150	50.9	19.7	8.3	7.7				

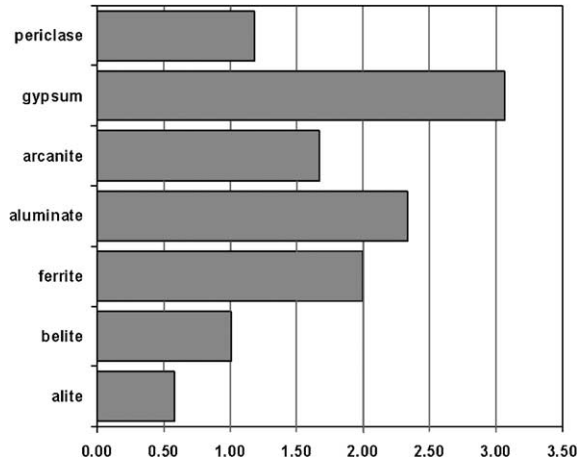

Fig. 10. Surface area to mass fraction ratio plot for averaged values of the six fields shows that the silicates have less surface area relative to the interstitial phases for this cement.

the bulk phase composition. SEM imaging and image analysis provide a means to make these measurements on cements. Comparison of bulk versus surface area mass fractions is provided in Fig. 9. Another means of examining this relationship is via a surface/bulk ratio plot as shown in Fig. 10. The difference in surface to bulk phase fraction reflects a combination of clinker texture and grinding characteristics. For cement #142, alite surface area is substantially lower relative to the bulk, belite is about equally represented, and the phases tricalcium aluminate, periclase, alkali sulfate and calcium sulfate exhibit greater surface area relative to the bulk. These relationships are the subject of additional study in a project to characterize the CCRL cements. The ability to better describe cement compositional and textural characteristics promises to make cements a more predictable material. Many of the cements analyzed are available online through VCCTL at http://vcctl.cbt.nist.gov/.

5. Conclusions

The knowledge of a bulk and surface phase composition of hydraulic cement should provide new insights into early-age hydration characteristics, cement–chemical admixture interactions, and aid in developing new hydraulic cements. These measurements are made possible through the imaging capabilities of the scanning electron microscope with imaging and X-ray microanalysis by:

1. backscattered electron SEM, combined with X-ray imaging provides the basis for a quantitative assessment of the phases in portland cement,
2. segmentation into the individual phases is achieved by a combination of imaging 'rules' and individual constituents may be highlighted using false color,
3. the resulting composite image can be analyzed to calculate volume percent, mass percent, and percentages based upon surface area measurements of the individual phases,
4. mass percentages obtained by this procedure are in good agreement with percentages based upon QXRD and may differ significantly from those estimated by the Bogue calculations, and
5. phase fractions by surface area show considerable difference from those expressed as bulk mass fractions. The finer-grained phases (gypsum, tricalcium aluminate, and ferrite) show much higher surface areas per unit mass than the coarser-grained phases such as alite and belite.

Acknowledgements

This project is supported by the High-Performance Concrete (HYPERCON) program at the Building and Fire Research Laboratory at the National Institute of Standards and Technology. The comments and suggestions of the Edward Garboczi and Jeff Bullard of NIST and the journal referees are gratefully acknowledged.

References

[1] Bogue RH. The chemistry of portland cement. 2nd ed. New York: Reinhold Publishing; 1955. 703 p.
[2] Standard test method for quantitative determination of phases in portland cement clinker by microscopical point-count procedure, ASTM C 1356. Annual book of ASTM standards, vol. 4.01, 2001.
[4] Bogue RH. Calculation of the compounds in portland cement. PCA fellowship paper no. 21, October, 1929. Also—Ind Eng Chem 1929;1(4):192.
[5] Taylor HFW. Cement chemistry. 2nd ed. Thomas Telford; 1997. 459 p.
[6] Campbell DH. Microscopical examination and interpretation of portland cement and clinker. 2nd ed. Portland Cement Association; 1999. 201 p.
[7] Hofmänner F. Microstructure of portland cement clinker. Holderbank, Switzerland: Holderbank Management and Consulting, Ltd.; 1973. 48 p.
[9] Harrison AM, Taylor HFW, Winter NB. Electron optical analyses of the phases in a portland cement clinker, with some observations on the calculation of quantitative phase composition. Cem Concr Res 1985;15:775.
[10] Gebauer J, Kristmann M. The influence of the composition of industrial clinker on cement and concrete properties. World Cem Technol 1979:46–51.
[11] Johansen V. Manufacturing processes and clinker performance. In: Young JF, editor. Characterization and performance prediction of cement and concrete, Proceedings of the Second Engineering Foundation Conference, 1983. p. 1–10.
[12] Miller G, Tang F. Cem Concr Res 1996;26(12):1821–9.

[13] Scrivner KL. The microstructure of anhydrous cement and its effect on hydration. In: Materials Research Society Symposium Proceedings, vol. 85, 1987. p. 39–46.
[14] Bentz DP, Stutzman PE. SEM analysis and computer modelling of hydration of portland cement particles. In: DeHayes SM, Stark D, editors. Petrography of Cementitious Materials. ASTM STP 1215. Philadelphia: American Society for Testing and Materials; 1994. p. 60–73.
[16] Goldstein JI, Newbury DE, Echlin P, Joy DC, Romig Jr D, Lyman CE, et al. Scanning electron microscopy and X-ray microanalysis. 2nd ed. New York: Plenum Press; 1992. 819 p.
[17] Stutzman PE, Clifton JR. Sample preparation for scanning electron microscopy. In: Jany L, Nisperos A, editors, Proceedings of the Twenty-First International Conference on Cement Microscopy, 25–29 April 1999. Las Vegas, Nevada, 1999. p. 10–22. Available from: http://ciks.cbt.nist.gov/~garbocz/icma1999/icma99.htm.
[18] Campbell DH, Galehouse JS. Quantitative clinker microscopy with the light microscope. Cem Concr Aggregates 1991;13(2):94–6 (American Society for Testing and Materials, Winter).
[19] Bentz D. The virtual cement and concrete testing laboratory. Available from: http://vcctl.cbt.nist.gov/.
[20] Stutzman PE, Leigh S. Phase composition analysis of the NIST reference clinkers by optical microscopy and X-ray powder diffraction. NIST technical note 1441, September 2002, 44 pp.